Deep Fourier Up-Sampling

Anonymous Author(s)
Affiliation
Address
email

Abstract

Existing convolutional neural networks widely adopt spatial down-/up-sampling for multi-scale modeling. However, spatial up-sampling operators (*e.g.*, interpolation, transposed convolution, and un-pooling) heavily depend on local pixel attention, incapably exploring the global dependency. In contrast, the Fourier domain is in accordance with the nature of global modeling according to the spectral convolution theorem. Unlike the spatial domain that easily performs up-sampling with the property of local similarity, up-sampling in the Fourier domain is more challenging as it does not follow such a local property. In this study, we propose a theoretically feasible Deep Fourier Up-Sampling (FourierUp) to solve these issues. We revisit the relationships between spatial and Fourier domains and reveal the transform rules on the features of different resolutions in the Fourier domain, which provide key insights for FourierUp's designs. FourierUp as a generic operator consists of three key components: 2D discrete Fourier transform, Fourier dimension increase rules, and 2D inverse Fourier transform, which can be directly integrated with existing networks. Extensive experiments across multiple computer vision tasks, including object detection, image segmentation, image de-raining, image dehazing, and guided image super-resolution, demonstrate the consistent performance gains obtained by introducing our FourierUp. Code will be publicly available.

1 Introduction

Motivation. The spatial down-/up-sampling has been widely used in convolutional neural networks for multi-scale modeling. For example, U-Net [1], a variation of encoder-decoder, utilizes pooling layers to reduce the feature resolution in the encoder and then recovers the resolution using up-sampling operations in the decoder. In addition, the feature pyramid [2–5] and image pyramid [6–9] driven multi-scale neural networks rely on the down-/up-sampling operation to obtain multi-scale property and improve modeling capability. However, spatial up-sampling operators (*e.g.*, interpolation, transposed convolution, and un-pooling) heavily depend on local pixel attention, and thus cannot explore the global dependency that is indispensable for many computer vision tasks [10, 11, 1, 12]. According to the spectral convolution theorem, the Fourier domain is in accordance with the nature of global modeling, which provides an alternative solution for multi-scale modeling. However, unlike the spatial domain with local similarity property, up-sampling in the Fourier domain is more challenging as it does not follow such a local property. This encourages us to explore deep Fourier up-sampling.

Recent studies have explored the information interaction in both spatial and Fourier domains. FFC [13], for instance, replaces the conventional convolution with a spatial-Fourier interaction, which consists of a spatial (or local) path that performs conventional convolution on a portion of input feature channels and a spectral (or global) path that operates in the Fourier domain. DFT [14] devises a Residual Fast Fourier Transform Block to integrate both low- and high-frequency residual information by performing the interaction between a regular spatial residual stream and a channel-wise Fourier

Submitted to 36th Conference on Neural Information Processing Systems (NeurIPS 2022). Do not distribute.

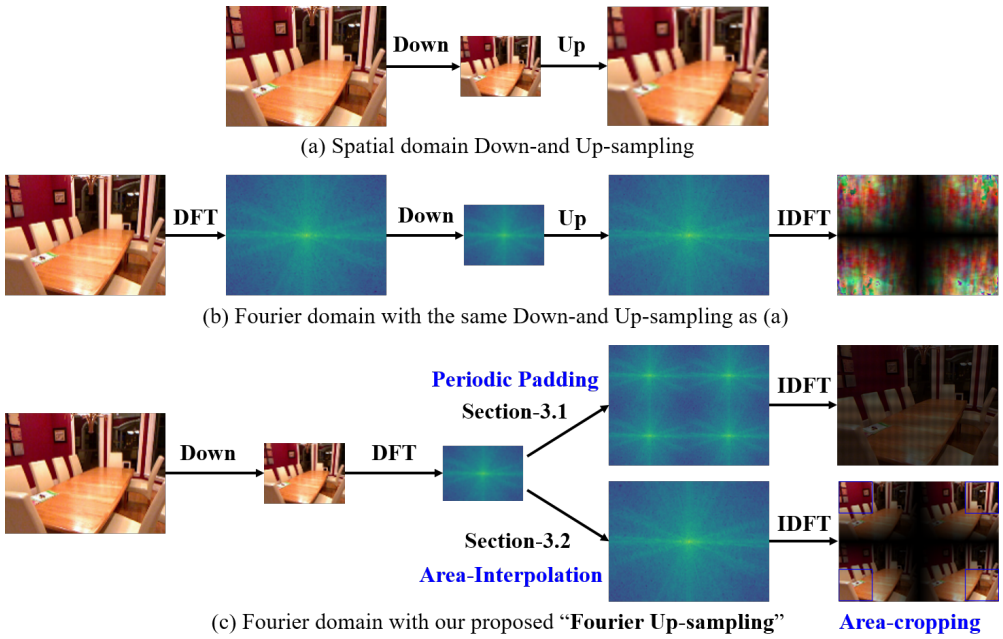

(a) Spatial domain Down-and Up-sampling

(b) Fourier domain with the same Down-and Up-sampling as (a)

(c) Fourier domain with our proposed "**Fourier Up-sampling**"

Figure 1: **An illustration of our motivation.** (a) and (b) imply that arbitrary up-sampling, *e.g.*, interpolation, in the Fourier domain produces sub-optimal result as it does not follow the same local similarity property as that in the spatial domain. *This motivates us to design a more ingenious "Fourier Up-Sampling" operator, dubbed as FourierUp. It has two alternative variants: Periodic Padding and Area Interpolation/Cropping, as illustrated in (c).*

transform stream. However, the aforementioned methodologies only interact at a single resolution scale, and the spatial-Fourier interaction potential of multiple scales in the Fourier domain has not been investigated. The key to solving this problem lies in how to implement deep Fourier up-sampling for multi-scale Fourier pattern modeling.

Challenges. We thus seek a potential solution for multi-scale Fourier pattern modeling by designing deep Fourier up-sampling. Owing to the local similarity and cross-scale position invariant properties of the spatial domain, the various spatial up-sampling operations including transposed convolution, un-pooling, and interpolation techniques are capable of using the pixel neighboring relationship to interpolate the unknown pixel values at local regions, increasing the spatial resolution of the features, as shown in Fig.1(a). In contrast to the spatial domain, the Fourier domain does not share the same scale-invariant property and local texture similarity, and hence cannot implement up-sampling using the same techniques as the spatial domain, as illustrated in Fig. 1(b). We therefore wonder "Can we provide a reliable up-sampling in the Fourier domain in a theoretical sound manner?".

Solutions. To answer this question, we first revisit the relationship between spatial and Fourier domains, revealing the transform rules on the features of different resolutions in the Fourier domain (see Section 3.2 and Section 3.3). On the basis of the above rules, we propose a theoretically feasible Deep Fourier Up-Sampling (FourierUp). Specifically, we develop two variants (Periodic Padding and Area Interpolation/Cropping) of FourierUp (see Section 3.4), as illustrated in Fig. 1(c). Each variant consists of three key components: 2D discrete Fourier transform, Fourier dimension increase rules, and 2D inverse Fourier transform. FourierUp is a generic operator that can be directly integrated with existing networks. Extensive experiments on multiple computer vision tasks, including object detection, image segmentation, image de-raining, image dehazing, and guided image super-resolution, demonstrate the consistent performance gains obtained by introducing our FourierUp. *We believe that the proposed FourierUp could refresh the neural network designs where the spatial and Fourier information interaction at only a single resolution scale previously reigned supreme.*

Contributions. 1) We propose a novel Deep Fourier Up-Sampling, which enables the integration of the features of different resolutions in the Fourier domain. To the best of our knowledge, this is the first thorough effort to explore the Fourier up-sampling for multi-scale modeling. 2) The proposed FourierUp is a generic operator that can be directly integrated with the existing networks, which provides flexible plug-and-play. 3) Equipped with the theoretically feasible FourierUp, the networks

achieve consistent performance improvement across multiple computer vision tasks, which suggests the potential of our method for refreshing the neural network designs in the Fourier domain.

2 Related Work

Spatial Up-Sampling. Convolutional neural networks with spatial down-/up-sampling have become the *de facto* structures in many computer vision tasks [15–23]. Typically, U-Net [1] builds multi-scale feature maps using the encoder with down-sampling and then utilizes the up-sampling operation to fuse the multi-scale features in the decoder. Additionally, the feature pyramid [2–5] and image pyramid[6–9] are commonly used to obtain the multi-scale property in neural networks [6–9]. Among them, spatial up-sampling plays a significant role in multi-scale modeling. However, existing up-sampling operations only work in the spatial domain and current studies rarely explore the potential (*e.g.*, the global modeling capability) of up-sampling in the frequency domain.

Spatial-Fourier Interaction. Recently, several studies attempt to employ Fourier transform in deep models [24–27, 13]. Some of these efforts use discrete Fourier transform to transfer the spatial features to the Fourier domain and then use frequency information to improve the performance of particular tasks [24, 26]. Another line is to use convolution theorem to speed up the models, such as using fast Fourier transform (FFT) [27, 13]. For example, FFC [13] replaces the convolution with the spatial-Fourier interaction. The work proposed in [28] uses spectral pooling to reduce feature resolution by truncating the frequency domain representation. However, all the techniques only interact with each other at a single spatial resolution and have not explored the interaction potential at multiple resolutions in both spatial and frequency domains as performing the frequency up-sampling is non-trivial. As a tentative exploration, we study the relationship between the spatial domain and Fourier domain and reveal the transform rules over the feature of different resolutions in the Fourier domain. This delivers the underlying insights for the designs of multi-scale Fourier modeling patterns, which has the potential of versatility for different network architectures.

3 Deep Fourier Up-Sampling

We first explore the mapping relationship between the spatial and Fourier domains, and then present two Deep Fourier Up-sampling modules, which can be easily equipped into a general network architecture to deliver the spectral knowledge underlying data. The construction of these two FourierUp modules are inspired from the following theoretical evidences.

3.1 Theoretical Evidences for FourierUp Module Construction

For a spacial map $g(x, y) \in \mathbb{R}^{M\times N}$, we denote its 2-times up-sampled dilated interpolation as $f_g^{dil}(x, y) \in \mathbb{R}^{2M\times 2N}$, with expression as

$$f_g^{dil}(x,y) \quad = \quad \begin{cases} g(\frac{x}{2}, \frac{y}{2}), & x = 2m, y = 2n \\ 0, & \text{others} \end{cases} \tag{1}$$

where $m = 0, 1, 2, \ldots, M-1$ and $n = 0, 1, 2, \ldots, N-1$. Denote $G(u, v) \in \mathbb{R}^{M\times N}$, $F_g^{dil}(u, v) \in \mathbb{R}^{2M\times 2N}$ as the corresponding Fourier transforms of g and f_g^{dil}, respectively.

In the spectral domain, denote the two-times up-sampled Periodic Padding interpolation of G as

$$F_G^{PP}(u + pM, v + qN) = G(u, v), \;\; p, q = 0, 1, u = 0, 1, \cdots, M, v = 0, 1, \cdots, N, \tag{2}$$

and denote its two-times up-sampled Area Interpolation as

$$F_G^{AI}(2u + p, 2v + q) = G(u, v), \;\; p, q = 0, 1, u = 0, 1, \cdots, M-1, v = 0, 1, \cdots, N-1. \tag{3}$$

Denote the inverse Fourier transform of F_G^{AI} as f_G^{AI}.

Theorem-1. For up-sampled Periodic Padding interpolation F_G^{PP} of the Fourier map G, it holds that $F_G^{PP}/4 = F_g^{dil}$.

This theorem implies that the spectral interpolation F_G^{PP} of G be exactly transformed to a type of spacial interpolation of the original map g (under a proportional constant decay). This naturally inspires to design Periodic Padding up-sampling scheme in spectral domain.

Theorem-2. For up-sampled Area Interpolation F_G^{AI} of G, for any $p, q = 0, 1$, it holds that

$$f_G^{AI}(x + pM, y + qN) = \frac{A((1-(-1)^p)M + (-1)^p x, (1-(-1)^q)M + (-1)^q y)}{4} g(x, y), \quad (4)$$

where $A(x, y) = 1 + e^{\frac{j\pi x}{M}} + e^{\frac{j\pi y}{N}} + e^{j\pi(\frac{x}{M}+\frac{y}{N})}$ and $x = 0, 1, \ldots M-1, y = 0, 1, \ldots N-1$.

This theorem implies that the spatial transform of the spectral interpolation F_G^{AI} of G is with an explicit relationship with the original spatial map g by a mapping A. A very good property of A, as depicted in Fig. 2, is that its intensity quickly drops to zero from the four map corders to its center. This inspires us to first crop these corners and then merge them to get the final Area Interpolation-Cropping Up-sampling scheme.

We first provide the proofs of the two theorems, and then introduce the design details of these two FourierUp modules.

3.2 Proof-1 of Theorem-1: Periodic Padding of Magnitude and Phase

Note that the relationship between $f_g^{dil}(x, y) \in \mathbb{R}^{2M \times 2N}$ and $g(x, y)$ can be written as

$$f_g^{dil}(x, y) \quad = \quad \begin{cases} g(\frac{x}{2}, \frac{y}{2}), & x = 2m, y = 2n \\ 0, & \text{others} \end{cases} \quad (5)$$

where $m = 0, 1, 2, \ldots, M-1$ and $n = 0, 1, 2, \ldots, N-1$. And the Fourier transform $F_g^{dil}(u, v)$ of $f_g^{dil}(x, y)$ is thus expressed as

$$\begin{aligned} F_g^{dil}(u, v) &= \frac{1}{4MN} \sum_{x=0}^{2M-1} \sum_{y=0}^{2N-1} f_g^{dil}(x, y) e^{-j2\pi(\frac{ux}{2M}+\frac{vy}{2N})} \\ &= \frac{1}{4MN} \sum_{x=0}^{M-1} \sum_{y=0}^{N-1} f_g^{dil}(2x, 2y) e^{-j2\pi(\frac{u(2x)}{2M}+\frac{v(2y)}{2N})} \\ &= \frac{1}{4MN} \sum_{x=0}^{M-1} \sum_{y=0}^{N-1} f_g^{dil}(2x, 2y) e^{-j2\pi(\frac{ux}{M}+\frac{vy}{N})} \\ &= \frac{1}{4MN} \sum_{x=0}^{M-1} \sum_{y=0}^{N-1} g(x, y) e^{-j2\pi(\frac{ux}{M}+\frac{vy}{N})}. \end{aligned} \quad (6)$$

Then, we show the periodicity of $F_g^{dil}(u, v) \in \mathbb{R}^{2M \times 2N}$ with M and N. It means $F_g^{dil}(u, v) = F_g^{dil}(u + M, v) = F_g^{dil}(u, v + N) = F_g^{dil}(u + M, v + N)$ with $u = 0, 1, 2, \ldots, M-1$ and $v = 0, 1, 2, \ldots, N-1$. We take the $F_g^{dil}(u, v) = F_g^{dil}(u + M, v)$ for example and recall Eq. (6) as

$$\begin{aligned} F_g^{dil}(u + M, v) &= \frac{1}{4MN} \sum_{x=0}^{M-1} \sum_{y=0}^{N-1} f_g^{dil}(2x, 2y) e^{-j2\pi(\frac{(u+M)x}{M}+\frac{vy}{N})} \\ &= \frac{1}{4MN} \sum_{x=0}^{M-1} \sum_{y=0}^{N-1} f_g^{dil}(2x, 2y) e^{-j2\pi(\frac{ux}{M}+\frac{vy}{N})} e^{-2j\pi x} \\ &= \frac{1}{4MN} \sum_{x=0}^{M-1} \sum_{y=0}^{N-1} f_g^{dil}(2x, 2y) e^{-j2\pi(\frac{ux}{M}+\frac{vy}{N})} \\ &= F_g^{dil}(u, v), \end{aligned} \quad (7)$$

where $e^{-2\pi jx} = 1$ for any integer x. Similarly, we can easily proof the periodicity of $F_g^{dil}(u, v)$.

Based on the above proof, the DFT of $g(x, y)$ can be formulated as

$$G(u, v) = \frac{1}{MN} \sum_{x=0}^{M-1} \sum_{y=0}^{N-1} g(x, y) e^{-j2\pi(\frac{ux}{M}+\frac{vy}{N})}. \quad (8)$$

Revising Eq. (6), we can figure out that $G(u, v) = \frac{F_g^{dil}(u,v)}{4}$.

3.3 Proof-2 of Theorem-2: Area Interpolation of Magnitude and Phase

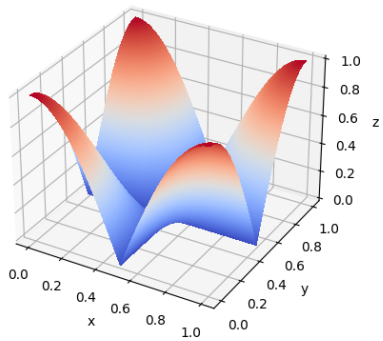

Figure 2: **The surface of $A(x, y)$.**

The 2D Inverse Discrete Fourier transform (IDFT) of $G(u, v)$ can be written as

$$g(x, y) = \frac{1}{MN} \sum_{u=0}^{M-1} \sum_{v=0}^{N-1} G(u, v) e^{j2\pi(\frac{ux}{M} + \frac{vy}{N})}. \tag{9}$$

We up-sample $G(u, v) \in \mathbb{R}^{M \times N}$ to get $F_G^{AI}(u, v) \in \mathbb{R}^{2M \times 2N}$. Specifically, the area interpolation shown in Fig. 4(b) is used for interpolation and then the interpolated pixels are the same as the original pixel in the 2×2 local regions. Namely, $F_G^{AI}(2u, 2v) = F_G^{AI}(2u + 1, 2v) = F_G^{AI}(2u, 2v + 1) = F_G^{AI}(2u + 1, 2v + 1) = G(u, v)$ with $u = 0, 1, \ldots, M - 1$ and $v = 0, 1, \ldots, N - 1$. Similar to Eq. (6), we can infer

$$\begin{aligned}
f_G^{AI}(x, y) &= \frac{1}{4MN} \sum_{u=0}^{2M-1} \sum_{v=0}^{2N-1} F_G^{AI}(u, v) e^{j2\pi(\frac{ux}{2M} + \frac{vy}{2N})} \\
&= \frac{1}{4MN} \sum_{u=0}^{M-1} \sum_{v=0}^{N-1} F_G^{AI}(2u, 2v) e^{j2\pi(\frac{2ux}{2M} + \frac{2vy}{2N})} + \frac{1}{4MN} \sum_{u=0}^{M-1} \sum_{v=0}^{N-1} F_G^{AI}(2u + 1, 2v) e^{j2\pi(\frac{(2u+1)x}{2M} + \frac{2vy}{2N})} \\
&+ \frac{1}{4MN} \sum_{u=0}^{M-1} \sum_{v=0}^{N-1} F_G^{AI}(2u, 2v + 1) e^{j2\pi(\frac{2ux}{2M} + \frac{(2v+1)y}{2N})} + \frac{1}{4MN} \sum_{u=0}^{M-1} \sum_{v=0}^{N-1} F_G^{AI}(2u + 1, 2v + 1) e^{j2\pi(\frac{(2u+1)x}{2M} + \frac{(2v+1)y}{2N})} \\
&= \frac{1}{4MN} \sum_{u=0}^{M-1} \sum_{v=0}^{N-1} G(u, v) e^{j2\pi(\frac{ux}{M} + \frac{vy}{N})} [1 + e^{\frac{j\pi x}{M}} + e^{\frac{j\pi y}{N}} + e^{j\pi(\frac{x}{M} + \frac{y}{N})}].
\end{aligned} \tag{10}$$

Similarly, we can write $g(x, y)$ as

$$g(x, y) = \frac{1}{MN} \sum_{u=0}^{M-1} \sum_{v=0}^{N-1} G(u, v) e^{j2\pi(\frac{ux}{M} + \frac{vy}{N})}. \tag{11}$$

Recalling Eq. (10) and Eq. (12), we can infer, for any $p, q = 0, 1$, it holds that

$$f_G^{AI}(x + pM, y + qN) = \frac{A((1 - (-1)^p)M + (-1)^p x, (1 - (-1)^q)M + (-1)^q y)}{4} g(x, y). \tag{12}$$

where $x = 0, 1, \ldots M - 1, y = 0, 1, \ldots N - 1$. Take the $p, q = 0$ for example, we can obtain $1 + e^{\frac{j\pi x}{M}} + e^{\frac{j\pi y}{N}} + e^{j\pi(\frac{x}{M} + \frac{y}{N})} = A(x, y)$, where

$$A(x, y) = (1 + \cos \pi \frac{x}{M} + \cos \pi \frac{y}{N} + \cos \pi (\frac{x}{M} + \frac{y}{N})) + j(\sin \pi \frac{x}{M} + \sin \pi \frac{y}{N} + \sin \pi (\frac{x}{M} + \frac{y}{N})), \tag{13}$$

and then

$$|A(x, y)|^2 = (1 + \cos \pi \frac{x}{M} + \cos \pi \frac{y}{N} + \cos \pi (\frac{x}{M} + \frac{y}{N}))^2 + (\sin \pi \frac{x}{M} + \sin \pi \frac{y}{N} + \sin \pi (\frac{x}{M} + \frac{y}{N}))^2. \tag{14}$$

We can find that the variable x shares the same operations as the variable y. For brevity, we only take the operation of variable x as example

$$\begin{aligned}
\frac{\partial |A(x, y)|^2}{\partial x} &= \frac{2\pi}{M} (1 + \cos \pi \frac{x}{M} + \cos \pi \frac{y}{N} + \cos \pi (\frac{x}{M} + \frac{y}{N}))(-\sin \pi \frac{x}{M} - \sin \pi (\frac{x}{M} + \frac{y}{N})) \\
&+ \frac{2\pi}{M} (\sin \pi \frac{x}{M} + \sin \pi \frac{y}{N} + \sin \pi (\frac{x}{M} + \frac{y}{N}))(\cos \pi (\frac{x}{M}) + \cos \pi (\frac{x}{M} + \frac{y}{N})) \\
&= -\frac{4\pi}{M} (\sin \pi \frac{x}{M})(1 + \cos \pi (\frac{y}{N})).
\end{aligned} \tag{15}$$

Equally, we have

$$\frac{\partial |A(x, y)|^2}{\partial y} = -\frac{4\pi}{N} \sin \pi \frac{y}{N} (1 + \cos \pi (\frac{x}{M})). \tag{16}$$

We prove that the partial derivative of $|A(x, y)|$ on both x and y are negative for $x = 0, 1, \ldots M - 1, y = 0, 1, \ldots N - 1$. Besides, we have

$$|A(x, y)| = |A(2M - x, y)| = |A(2M, 2N - y)| = |A(2M - x, 2N - y)|. \tag{17}$$

That is to say, the intensity drops from the side to the center, shown in Fig. 2. Specifically, the intensity drops to zero at the position of $x = M$ or $y = N$.

```
def FourierUp_Padding(X):
 # X: input with shape [N, C, H, W]
 # A and P are the amplitude and phase
    A, P = FFT(X)

    # Fourier up-sampling transform
        rules
    A_pep = Periodic-Padding(A)
    P_pep = Periodic-Padding(P)
    A_pep = Convs_1x1(A_pep)
    P_pep = Convs_1x1(P_pep)

    # Inverse Fourier transform
    Y = iFFT(A_pep, P_pep)

    Return Y #[N, C, 2H, 2W]
```

```
def FourierUp_AreaInterpolation(X):
 # X: input with shape [N, C, H, W]
 # A and P are the amplitude and phase
    A, P = FFT(X)

    # Fourier up-sampling transform rules
    A_aip = Area-Interpolation(A)
    P_aip = Area-Interpolation(P)
    A_aip = Convs_1x1(A_aip)
    P_aip = Convs_1x1(P_aip)

    # Inverse Fourier transform
    Y = iFFT(A_aip, P_aip)

    #Area Cropping
    Y = Area-Cropping(Y)
    Y = Resize(Y)

    Return Y #[N, C, 2H, 2W]
```

Figure 3: **Pseudo-code of the two variants of the proposed deep Fourier up-sampling.** The left is the *periodic padding variant* while the right is the *area interpolation-cropping variant*.

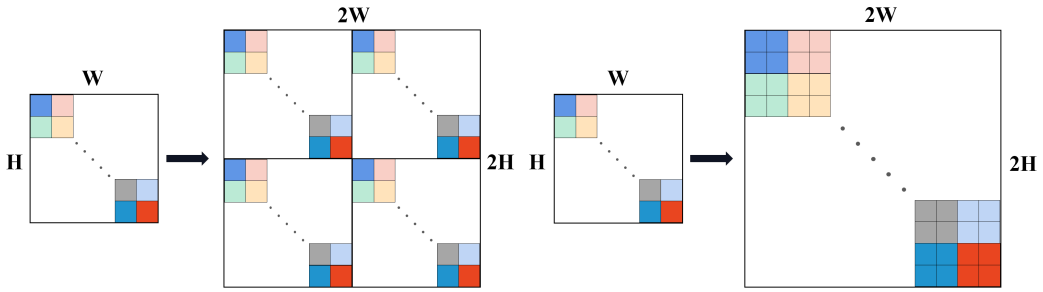

(a) Periodic Padding (b) Area Interpolation

Figure 4: **The illustrations of (a) periodic padding and (b) area interpolation in Figure 3.** Each small color square represents a pixel of the amplitude/phase component in the Fourier domain.

3.4 FourierUp Module Design

Recalling **Theorem-1** and **Theorem-2**, we correspondingly propose two deep Fourier up-sampling models, called Periodic Padding and Area Interpolation-Cropping, respectively.

Periodic Padding Up-Sampling. The pseudo-code of the Periodic Padding Up-Sampling scheme is shown in the left part of Fig. 3. Specifically, given an image $\mathrm{X} \in \mathbb{R}^{\mathrm{H} \times \mathrm{W} \times \mathrm{C}}$, we first adopt the Fourier transform $\mathrm{FFT}(\mathrm{X})$ to obtain its amplitude component A and phase component P. We then perform the periodic padding over A and P two times in both the H and W dimensions, as illustrated in Fig. 4(a), to form the padded $\mathrm{A_pep}$ and $\mathrm{P_pep}$. Such up-sampling maps are then fed into two independent convolution module with a kernel size of 1×1 and followed by the inverse Fourier transform $\mathrm{iFFT}(.)$ to project the padded ones back to the spatial domain.

Area Interpolation-Cropping Up-Sampling. The pseudo-code of Area interpolation-Cropping Up-Sampling module is shown in the right part of Fig. 3. We first conduct the Area interpolation over the phase and amplitude by 2×2 area interpolation with the same pixel, as illustrated in Fig. 4(b). We then employ the inverse Fourier transform to project the interpolated ones back to the spatial domain. As described in section 3.3, the inverse spatial representation is periodic while the pixel value tends to be decayed quickly. The degree of decay of the pixel increases when the pixel is closer to the center. To better maintain the information, we perform the area cropping operation (detailed in Fig. 1) in the four corners with the $\frac{W}{2} \times \frac{H}{2}$ size, then merge them together as a whole at the spatial dimension, and finally resize them to the expected up-sampling scale of $2H \times 2W$.

4 Experiments

To demonstrate the efficacy of our proposed deep Fourier up-sampling, we conduct extensive experiments on multiple computer vision tasks, including object detection, image segmentation, image de-raining, image dehazing, and guided image super-resolution. We provide more experimental results in the supplementary material.

4.1 Experimental Settings

Object Detection. Following [12], the PASCAL VOC 2007 and 2012 training sets [29] are used as training data. The PASCAL VOC 2007 testing set is used for evaluations as the ground truth annotations of VOC 2012 testing set are not publicly available. We employ the FPN-based Faster RCNN [12] with ResNet50 backbone and YOLO-v3 with Darknet53 [30] as baselines.

Image Segmentation. Following [31, 32], Synapse Dataset and CANDI Dataset are used as the testbed of medical image segmentation. We adopt the two representative image segmentation algorithms, U-Net [1] and Att-UNet [33], as the base models.

Image De-raining. Following [34], we choose two widely-used standard benchmark datasets, including Rain200H and Rain200L, for evaluations. we employ two representative de-raining methods, LPNet with up-sampling [11] and PReNet without up-sampling [34], as baselines.

Image Dehazing. Following [10], we employ RESIDE[35] dataset [36] for evaluations. We also use two different network designs AODNet [37] without up-sampling operator and MSBDN [10] with up-sampling operator, for validation.

Guided Image Super-resolution. Following [38, 39], we adopt the pan-sharpening, the representative task of guided image super-resolution, for evaluations. The WorldView II, WorldView III, and GaoFen2 in [38, 39] are used for evaluations. We employ two different network designs for validation, including PANNET [40] without up-sampling operator and DCFNET [41] with up-sampling operator.

Several widely-used image quality assessment (IQA) metrics are employed to evaluate the performance, including the relative dimensionless global error in synthesis (ERGAS) [42], the peak signal-to-noise ratio (PSNR), the spectral angle mapper (SAM) [43], DSC, and HD95.

4.2 Implementation Details

Regarding the above competitive baselines, they can be divided into two categories: one with spatial up-sampling ([1], Att-UNet [33], DCFNET [41], LPNet [11], MSBDN [10]) and another one without spatial up-sampling (PReNet [34], AODNet[37], PANNET [40]). The purpose of the exploration on the baselines without spatial up-sampling is to show the versatility of our FourierUp for different network structures. Different from directly replacing the spatial up-sampling with the FourierUp in the baselines with spatial up-sampling, we need to encapsulate the FourierUp for the baselines without spatial up-sampling, in which a down-sampling operation is introduced to first reduce the resolution of features. We provide the detailed structures of the encapsulated FourierUp and the baselines with the FourierUp in the supplementary material.

For the baselines with spatial up-sampling, we perform the comparison over four configurations:

1) **Original**: the baseline without any changes;
2) **FourierUp-AreaUp**: replacing the original model's spatial up-sampling with the union of the Area-Interpolation variant of our FourierUp and the spatial up-sampling itself;
3) **FourierUp-Padding**: replacing the original model's spatial up-sampling operator with the union of the Periodic-Padding variant of our FourierUp and the spatial up-sampling itself;
4) **Spatial-Up**: replacing the variants of FourierUp in the settings of $2)/3)$ with the spatial up-sampling. For a fair comparison, we use the same number of trainable parameters as $2)/3)$.

For the baselines without spatial up-sampling, we perform the comparison over four configurations:

1) **Original**: the baseline without any changes;
2) **FourierUp-AreaUp**: replacing the original model's convolution with the encapsulated FourierUp that is equipped with the Area-Interpolation variant;

3) **FourierUp-Padding**: replacing the original model's convolution with the encapsulated FourierUp that is equipped with the Periodic-Padding variant;
4) **Spatial-Up**: replacing the the encapsulated FourierUp of the settings of $2)/3)$ with the spatial up-sampling. For a fair comparison, we use the same number of trainable parameters as $2)/3)$.

Table 1: **Quantitative comparisons of image de-raining.**

Model	Configurations	Rain200H		Rain200L	
		PSNR	SSIM	PSNR	SSIM
LPNet	Original	22.907	0.775	32.461	0.947
	Spatial-Up	22.956	0.777	32.522	0.950
	FourierUp-AreaUp	22.163	0.783	32.681	0.954
	FourierUp-Padding	**23.295**	**0.786**	**32.835**	**0.956**
PReNet	Original	29.041	0.891	37.802	0.981
	Spatial-Up	29.357	0.901	38.271	0.985
	FourierUp-AreaUp	29.690	0.903	39.776	0.985
	FourierUp-Padding	**29.871**	**0.908**	**39.971**	**0.987**

Table 2: **Comparison over image dehazing.**

Model	configurations	PSNR	SSIM
AODNet	Original	18.80	0.834
	Spatial-Up	18.91	0.838
	FourierUp-AreaUp	19.16	0.843
	FourierUp-Padding	**19.35**	**0.847**
MSBDN	Original	33.79	0.984
	Spatial-Up	33.90	0.984
	FourierUp-AreaUp	34.21	0.985
	FourierUp-Padding	**34.35**	**0.987**

Table 3: **Comparison over object detection.**

Model	Methods	AP50	mAP
Faster RCNN	Original	79.13	79.10
	Spatial-Up	79.14	79.10
	FourierUp-AreaUp	79.17	79.14
	FourierUp-Padding	**79.21**	**79.16**
YOLO-V3	Original	81.68	81.63
	Spatial-Up	81.68	81.63
	FourierUp-AreaUp	81.73	81.71
	FourierUp-Padding	**81.77**	**81.74**

Table 4: **Quantitative comparisons of medical image segmentation.**

Model	Configurations	synapse		CANDI	
		DSC ↑	HD95 ↓	DSC ↑	HD95 ↓
U-Net	Original	76.85	39.70	86.50	3.946
	Spatial-Up	76.94	38.59	86.59	3.826
	FourierUp-AreaUp	77.25	36.02	86.63	3.751
	FourierUp-Padding	**77.37**	**35.86**	**86.70**	**3.327**
Att-UNet	Original	77.77	36.02	86.29	5.601
	Spatial-Up	77.85	35.91	86.35	5.588
	FourierUp-AreaUp	78.11	34.54	86.50	4.851
	FourierUp-Padding	**78.34**	**34.29**	**86.64**	**4.833**

Table 5: **Quantitative comparisons of pan-sharpening.**

Model	Configurations	WorldView-II				GaoFen2			
		PSNR↑	SSIM↑	SAM↓	ERGAS↓	PSNR↑	SSIM↑	SAM↓	EGAS↓
PANNET	Original	40.817	0.963	0.025	1.055	43.066	0.968	0.018	0.855
	Spatial-Up	40.988	0.963	0.025	1.031	43.897	0.973	0.018	0.737
	FourierUp-AreaUp	41.167	0.963	0.024	1.010	45.964	0.979	0.015	0.653
	FourierUp-Padding	**41.288**	**0.965**	**0.024**	**1.007**	**46.145**	**0.982**	**0.012**	**0.622**
DCFNET	Original	40.276	0.968	0.028	1.051	42.986	0.967	0.019	0.858
	Spatial-Up	40.319	0.968	0.028	**1.046**	43.157	0.970	0.017	0.850
	FourierUp-AreaUp	40.484	0.968	0.025	1.115	43.881	0.979	0.014	0.829
	FourierUp-Padding	**40.546**	**0.968**	**0.025**	1.102	**44.153**	**0.981**	**0.014**	**0.765**

4.3 Comparison and Analysis

Quantitative Comparison. We perform the model performance comparison over different configurations, as described in implementation details. The quantitative results are presented in Tables 1 to 5 where the best and second best results are highlighted in bold and Underline. From the results, by integrating with our proposed two FourierUp variants, we can observe performance gain against the baselines across all the datasets in all tested tasks, suggesting the effectiveness of our approach. For example, for the PReNet of Table 1, "FourierUp-padding" and "FourierUp-AreaUp" obtain 0.83dB/0.65dB and 2.1dB/1.9dB PSNR gains than the "Original", 0.52dB/0.34dB and 1.7dB/1.5dB PSNR gains than "Spatial-Up" on the Rain200H and Rain200L datasets, respectively. Such results

validate the effectiveness of our proposed FourierUp. The corresponding visualization consistently supports the analysis in Fig. 5, where the FourierUp is capable of better maintaining the details.

Qualitative Comparison. Due to the limited space, we only report the visual results of the de-raining/dehazing task in Fig. 5 and 6 that can more clearly show the effectiveness of FourierUp. More results can be found in the supplementary materials. As shown, integrating the FourierUp with the original baseline achieves more visually pleasing results. Specifically, zooming-in the red box region of Fig. 5 and 6, the model equipped with the FourierUp is capable of better recovering the texture details while removing the rain/hazy effect.

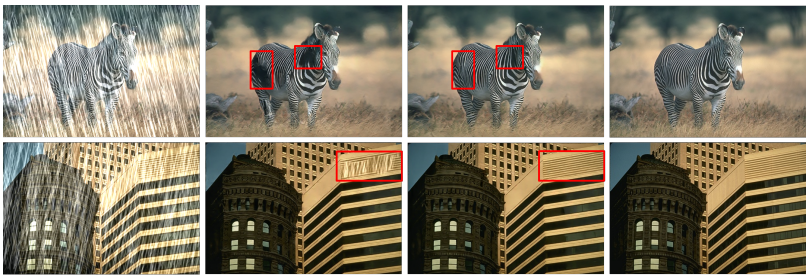

(a) Rainy image (b) PReNet (c) PReNet with FourierUp (d) Ground truth

Figure 5: **Visual comparison of PReNet on the Rain200H.**

(a) Hazy image (b) AODNet (c) AODNet with FourierUp (d) Ground truth

Figure 6: **Visual comparison of AODNet on the SOTS.**

5 Limitations

First, the more comprehensive experiments on broader computer vision tasks (*e.g.*, image de-noising and image classification) have not been explored. Second, the deep Fourier Up-sampling integrated with spatial up-sampling will increase the model parameter numbers. This is negligible at the significant performance gain at fewer parameter increase. Note that, the focus of this work is beyond designing a plug-and-play module to integrate it into existing networks for further performance gain. This work also provides a powerful scale change choice of the up-sampling operator pool when developing a new model from start.

6 Conclusion

In this paper, we have proposed a deep Fourier up-sampling to explore the possibility of the up-sampling in the Fourier domain, which provides the key insight for the multi-scale Fourier pattern modeling. We theoretically demonstrate that our designs of Fourier up-sampling are feasible. It is appealing that the proposed FourierUp is a generic operator, thus being directly integrated with existing networks. Extensive experiments demonstrate the effectiveness of our method. We believe the FourierUp has the potential to advance broader computer vision tasks, *e.g.*, image/video super-resolution and image/video in-painting.

Broader Impact

Our work shows the promising capability of up-sampling in the Fourier domain for computer vision algorithms through two novel designs with theoretical proofs. Using our deep Fourier up-sampling with negligible computational cost will improve the performance of neural networks and facilitate the development of AI in real-world applications. However, the efficacy of our method may raise potential concerns when it is improperly used. For example, the safety of the applications of our method in real-world applications may not be guaranteed. We will investigate the robustness and effectiveness of our method in broader real-world applications.

References

[1] Olaf Ronneberger, Philipp Fischer, and Thomas Brox. U-net: Convolutional networks for biomedical image segmentation. In *International Conference on Medical image computing and computer-assisted intervention*, pages 234–241. Springer, 2015.

[2] Tsung-Yi Lin, Piotr Dollár, Ross Girshick, Kaiming He, Bharath Hariharan, and Serge Belongie. Feature pyramid networks for object detection. In *Proceedings of the IEEE conference on computer vision and pattern recognition*, pages 2117–2125, 2017.

[3] Seung-Wook Kim, Hyong-Keun Kook, Jee-Young Sun, Mun-Cheon Kang, and Sung-Jea Ko. Parallel feature pyramid network for object detection. In *Proceedings of the European Conference on Computer Vision (ECCV)*, pages 234–250, 2018.

[4] Selim Seferbekov, Vladimir Iglovikov, Alexander Buslaev, and Alexey Shvets. Feature pyramid network for multi-class land segmentation. In *Proceedings of the IEEE Conference on Computer Vision and Pattern Recognition Workshops*, pages 272–275, 2018.

[5] Lei Zhu, Zijun Deng, Xiaowei Hu, Chi-Wing Fu, Xuemiao Xu, Jing Qin, and Pheng-Ann Heng. Bidirectional feature pyramid network with recurrent attention residual modules for shadow detection. In *Proceedings of the European Conference on Computer Vision (ECCV)*, pages 121–136, 2018.

[6] Yanwei Pang, Tiancai Wang, Rao Muhammad Anwer, Fahad Shahbaz Khan, and Ling Shao. Efficient featurized image pyramid network for single shot detector. In *Proceedings of the IEEE/CVF Conference on Computer Vision and Pattern Recognition*, pages 7336–7344, 2019.

[7] Ziming Liu, Guangyu Gao, Lin Sun, and Li Fang. Ipg-net: Image pyramid guidance network for small object detection. In *Proceedings of the IEEE/CVF Conference on Computer Vision and Pattern Recognition Workshops*, pages 1026–1027, 2020.

[8] Edward H Adelson, Charles H Anderson, James R Bergen, Peter J Burt, and Joan M Ogden. Pyramid methods in image processing. *RCA engineer*, 29(6):33–41, 1984.

[9] Jiapeng Luo, Jiaying Liu, Jun Lin, and Zhongfeng Wang. A lightweight face detector by integrating the convolutional neural network with the image pyramid. *Pattern Recognition Letters*, 133:180–187, 2020.

[10] Hang Dong, Jinshan Pan, Lei Xiang, Zhe Hu, Xinyi Zhang, Fei Wang, and Ming-Hsuan Yang. Multi-scale boosted dehazing network with dense feature fusion. In *2020 IEEE/CVF Conference on Computer Vision and Pattern Recognition (CVPR)*, pages 2154–2164, 2020.

[11] Xueyang Fu, Borong Liang, Yue Huang, Xinghao Ding, and John Paisley. Lightweight pyramid networks for image deraining. *IEEE Transactions on Neural Networks and Learning Systems*, 31(6):1794–1807, 2020.

[12] Shaoqing Ren, Kaiming He, Ross Girshick, and Jian Sun. Faster r-cnn: Towards real-time object detection with region proposal networks. *IEEE Transactions on Pattern Analysis and Machine Intelligence*, 39(6):1137–1149, 2017.

[13] Lu Chi, Borui Jiang, and Yadong Mu. Fast fourier convolution. In H. Larochelle, M. Ranzato, R. Hadsell, M. F. Balcan, and H. Lin, editors, *Advances in Neural Information Processing Systems*, 2020.

[14] Xintian Mao, Yiming Liu, Wei Shen, Qingli Li, and Yan Wang. Deep residual fourier transformation for single image deblurring. *arXiv preprint arXiv:2111.11745*, 2021.

[15] Yulun Zhang, Huan Wang, Can Qin, and Yun Fu. Aligned structured sparsity learning for efficient image super-resolution. *Advances in Neural Information Processing Systems*, 34, 2021.

[16] Yulun Zhang, Kunpeng Li, Kai Li, Gan Sun, Yu Kong, and Yun Fu. Accurate and fast image denoising via attention guided scaling. *IEEE Transactions on Image Processing*, 30:6255–6265, 2021.

[17] Yuchen Fan, Jiahui Yu, Yiqun Mei, Yulun Zhang, Yun Fu, Ding Liu, and Thomas S Huang. Neural sparse representation for image restoration. *Advances in Neural Information Processing Systems*, 33:15394–15404, 2020.

[18] Wenqi Ren, Jiawei Zhang, Jinshan Pan, Sifei Liu, Jimmy Ren, Junping Du, Xiaochun Cao, and Ming-Hsuan Yang. Deblurring dynamic scenes via spatially varying recurrent neural networks. *IEEE transactions on pattern analysis and machine intelligence*, 2021.

[19] Wenqi Ren, Jiawei Zhang, Lin Ma, Jinshan Pan, Xiaochun Cao, Wangmeng Zuo, Wei Liu, and Ming-Hsuan Yang. Deep non-blind deconvolution via generalized low-rank approximation. *Advances in neural information processing systems*, 31, 2018.

[20] He Zhang and Vishal M Patel. Density-aware single image de-raining using a multi-stream dense network. In *Proceedings of the IEEE conference on computer vision and pattern recognition*, pages 695–704, 2018.

[21] He Zhang, Vishwanath Sindagi, and Vishal M Patel. Image de-raining using a conditional generative adversarial network. *IEEE transactions on circuits and systems for video technology*, 30(11):3943–3956, 2019.

[22] Jinshan Pan, Sifei Liu, Deqing Sun, Jiawei Zhang, Yang Liu, Jimmy Ren, Zechao Li, Jinhui Tang, Huchuan Lu, Yu-Wing Tai, et al. Learning dual convolutional neural networks for low-level vision. In *Proceedings of the IEEE conference on computer vision and pattern recognition*, pages 3070–3079, 2018.

[23] Zongsheng Yue, Hongwei Yong, Qian Zhao, Deyu Meng, and Lei Zhang. Variational denoising network: Toward blind noise modeling and removal. In *Advances in Neural Information Processing Systems*, volume 32, 2019.

[24] Yanchao Yang and Stefano Soatto. Fda: Fourier domain adaptation for semantic segmentation, 2020.

[25] Shaohua Li, Kaiping Xue, Bin Zhu, Chenkai Ding, Xindi Gao, David Wei, and Tao Wan. Falcon: A fourier transform based approach for fast and secure convolutional neural network predictions. In *Proceedings of the IEEE/CVF Conference on Computer Vision and Pattern Recognition*, pages 8705–8714, 2020.

[26] Jae-Han Lee, Minhyeok Heo, Kyung-Rae Kim, and Chang-Su Kim. Single-image depth estimation based on fourier domain analysis. In *Proceedings of the IEEE Conference on Computer Vision and Pattern Recognition*, pages 330–339, 2018.

[27] Caiwen Ding, Siyu Liao, Yanzhi Wang, Zhe Li, Ning Liu, Youwei Zhuo, Chao Wang, Xuehai Qian, Yu Bai, Geng Yuan, et al. Circnn: accelerating and compressing deep neural networks using block-circulant weight matrices. In *Proceedings of the 50th Annual IEEE/ACM International Symposium on Microarchitecture*, pages 395–408, 2017.

[28] Oren Rippel, Jasper Snoek, and Ryan P Adams. Spectral representations for convolutional neural networks. *Advances in neural information processing systems*, 28, 2015.

[29] M. Everingham, L. V. Gool, Cki Williams, J. Winn, and A. Zisserman. The pascal visual object classes (voc) challenge. *International Journal of Computer Vision*, 88(2):303–338, 2010.

[30] Mingxing Tan, Ruoming Pang, and Quoc V. Le. Efficientdet: Scalable and efficient object detection. In *2020 IEEE/CVF Conference on Computer Vision and Pattern Recognition (CVPR)*, pages 10778–10787, 2020.

[31] Jieneng Chen, Yongyi Lu, Qihang Yu, Xiangde Luo, Ehsan Adeli, Yan Wang, Le Lu, Alan L Yuille, and Yuyin Zhou. Transunet: Transformers make strong encoders for medical image segmentation. *arXiv preprint arXiv:2102.04306*, 2021.

[32] Shuhao Fu, Yongyi Lu, Yan Wang, Yuyin Zhou, Wei Shen, Elliot Fishman, and Alan Yuille. Domain adaptive relational reasoning for 3d multi-organ segmentation. In *International Conference on Medical Image Computing and Computer-Assisted Intervention*, pages 656–666. Springer, 2020.

[33] Ozan Oktay, Jo Schlemper, Loic Le Folgoc, Matthew Lee, Mattias Heinrich, Kazunari Misawa, Kensaku Mori, Steven McDonagh, Nils Y Hammerla, Bernhard Kainz, et al. Attention u-net: Learning where to look for the pancreas. *arXiv preprint arXiv:1804.03999*, 2018.

[34] Dongwei Ren, Wangmeng Zuo, Qinghua Hu, Pengfei Zhu, and Deyu Meng. Progressive image deraining networks: A better and simpler baseline. In *Proceedings of the IEEE/CVF Conference on Computer Vision and Pattern Recognition (CVPR)*, June 2019.

[35] Boyi Li, Wenqi Ren, Dengpan Fu, Dacheng Tao, Dan Feng, Wenjun Zeng, and Zhangyang Wang. Benchmarking single-image dehazing and beyond. *IEEE Transactions on Image Processing*, 28(1):492–505, 2019.

[36] Yanfu Zhang, Li Ding, and Gaurav Sharma. Hazerd: An outdoor scene dataset and benchmark for single image dehazing. In *2017 IEEE International Conference on Image Processing (ICIP)*, pages 3205–3209, 2017.

[37] Boyi Li, Xiulian Peng, Zhangyang Wang, Jizheng Xu, and Dan Feng. Aod-net: All-in-one dehazing network. In *Proceedings of the IEEE International Conference on Computer Vision (ICCV)*, Oct 2017.

[38] Man Zhou, Xueyang Fu, Jie Huang, Feng Zhao, Aiping Liu, and Rujing Wang. Effective pan-sharpening with transformer and invertible neural network. *IEEE Transactions on Geoscience and Remote Sensing*, 60:1–15, 2022.

[39] Keyu Yan, Man Zhou, Liu Liu, Chengjun Xie, and Danfeng Hong. When pansharpening meets graph convolution network and knowledge distillation. *IEEE Transactions on Geoscience and Remote Sensing*, 60:1–15, 2022.

[40] Junfeng Yang, Xueyang Fu, Yuwen Hu, Yue Huang, Xinghao Ding, and John Paisley. Pannet: A deep network architecture for pan-sharpening. In *IEEE International Conference on Computer Vision*, pages 5449–5457, 2017.

[41] Xiao Wu, Ting-Zhu Huang, Liang-Jian Deng, and Tian-Jing Zhang. Dynamic cross feature fusion for remote sensing pansharpening. In *Proceedings of the IEEE/CVF International Conference on Computer Vision (ICCV)*, pages 14687–14696, October 2021.

[42] L. Alparone, L. Wald, J. Chanussot, C. Thomas, P. Gamba, and L. M. Bruce. Comparison of pansharpening algorithms: Outcome of the 2006 grs-s data fusion contest. *IEEE Transactions on Geoscience and Remote Sensing*, 45(10):3012–3021, 2007.

[43] A. F. Goetz J. R. H. Yuhas and J. M. Boardman. Discrimination among semi-arid landscape endmembers using the spectral angle mapper (sam) algorithm. *Proc. Summaries Annu. JPL Airborne Geosci. Workshop*, pages 147–149, 1992.

Checklist

1. For all authors...
   (a) Do the main claims made in the abstract and introduction accurately reflect the paper's contributions and scope? [Yes]
   (b) Did you describe the limitations of your work? [Yes] , see Section 5.
   (c) Did you discuss any potential negative societal impacts of your work? [Yes] , see Section 6.
   (d) Have you read the ethics review guidelines and ensured that your paper conforms to them? [Yes]
2. If you are including theoretical results...
   (a) Did you state the full set of assumptions of all theoretical results? [Yes] , See Section 3.2 and Section 3.3.
   (b) Did you include complete proofs of all theoretical results? [Yes] , See Section 3.2 and Section 3.3.

3. If you ran experiments...
   (a) Did you include the code, data, and instructions needed to reproduce the main experimental results (either in the supplemental material or as a URL)? [Yes]
   (b) Did you specify all the training details (e.g., data splits, hyperparameters, how they were chosen)? [Yes]
   (c) Did you report error bars (e.g., with respect to the random seed after running experiments multiple times)? [No] , the effect of random seed could almost be negligible since we set the same initiation seed during experiments. Reproducibility can be guaranteed.
   (d) Did you include the total amount of compute and the type of resources used (e.g., type of GPUs, internal cluster, or cloud provider)? [Yes]
4. If you are using existing assets (e.g., code, data, models) or curating/releasing new assets...
   (a) If your work uses existing assets, did you cite the creators? [Yes]
   (b) Did you mention the license of the assets? [Yes]
   (c) Did you include any new assets either in the supplemental material or as a URL? [Yes]
   (d) Did you discuss whether and how consent was obtained from people whose data you're using/curating? [Yes] , the data creators claim that they allow and encourage the data for scientific research.
   (e) Did you discuss whether the data you are using/curating contains personally identifiable information or offensive content? [N/A] , We train and test the framework using the publicly accessible datasets.
5. If you used crowdsourcing or conducted research with human subjects...
   (a) Did you include the full text of instructions given to participants and screenshots, if applicable? [N/A]
   (b) Did you describe any potential participant risks, with links to Institutional Review Board (IRB) approvals, if applicable? [N/A]
   (c) Did you include the estimated hourly wage paid to participants and the total amount spent on participant compensation? [N/A]